INTERNATIONAL JOURNAL OF
NUMERICAL ANALYSIS AND MODELING
Volume 9, Number 3, Pages 725–744

TREATMENT OF TENSORIAL RELATIVE PERMEABILITIES WITH MULTIPOINT FLUX APPROXIMATION

MARKUS WOLFF, BERND FLEMISCH, RAINER HELMIG, AND IVAR AAVATSMARK

Abstract. Multi-phase flow in porous media is most commonly modeled by adding a saturation-dependent, scalar relative permeability into the Darcy equation. However, in the general case anisotropically structured heterogeneities result in anisotropy of upscaled parameters, which not only depends on the solid structure but also on fluid-fluid or fluid-fluid-solid interaction. We present a method for modeling of incompressible, isothermal, immiscible two-phase flow, which accounts for anisotropic absolute as well as relative permeabilities. It combines multipoint flux approximation (MPFA) with an appropriate upwinding strategy in the framework of a sequential solution algorithm. Different tests demonstrate the capabilities of the method and motivate the relevance of anisotropic relative permeabilities. Therefore, a porous medium is chosen, which is heterogeneous but isotropic on a fine scale and for which averaged homogeneous but anisotropic parameters are known. Comparison shows that the anisotropy in the large-scale parameters is well accounted for by the method and agrees with the anisotropic distribution behavior of the fine-scale solution. This is demonstrated for both the advection dominated as well as the diffusion dominated case. Further, it is shown that off-diagonal entries in the relative permeability tensor can have a significant influence on the fluid distribution.

Key words. porous media, two-phase flow, anisotropic medium, anisotropy, tensorial relative permeability, MPFA, upwinding, capillary pressure, gravity

1. Introduction

Multi-phase flow and transport phenomena in porous media are the governing processes in many relevant systems. An example for a natural system is the subsurface, considering for example the remediation of non-aqueous phase liquids or modeling of CO_2 storage scenarios (e.g. [15]). Biological systems can for example be found in the human body, where flow through the brain or in the lung can be modeled as flow through porous media (e.g. [36, 23, 20]), and there also exist many technical applications in which multi-phase flow through porous media is important (e.g. [9, 8]).

Flow and transport processes in permeable media occur on different spatial scales and are in general highly affected by heterogeneities. Usually, averaged equations applying an REV (Representative Elementary Volume) concept are used, where the most common model is the so-called Darcy equation.This model can be used for single phase flow as well as for multi-phase flow. Parameters of averaged equations usually directly (analytical methods, averaging methods, etc.) or indirectly (e.g. experiments, measurements, etc.) imply an upscaling of processes which occur on smaller scales. If upscaling methods are applied to flow in porous media with distinctive anisotropically structured block heterogeneities, a direction dependence of the upscaled large-scale parameters results. It is fairly common to assume and determine anisotropic absolute permeabilities on various scales. Anisotropic phase-dependent behavior is often neglected in the upscaling process. However, it has been observed at different scales that upscaling can also lead to phase-dependent anisotropic full-tensor effects (e.g. [34, 10, 18]). These can either be treated in a

Received by the editors , 2011 and, in revised form, , 2011.
2000 *Mathematics Subject Classification.* 35R35, 49J40, 60G40.

classical sense by deriving anisotropic phase-dependent parameters like phase and relative permeabilities respectively [33] or by upscaling strategies which are more closely linked to a certain discretization method and account for full-tensor effects by incorporating global effects into isotropic upscaled parameters (e.g. [14, 27]). We will further focus on the former. If the principal directions of an upscaled total permeability coincide with the directions of a cartesian computational grid, the extension of a basic finite volume scheme is quite obvious. In that case, it just has to be distinguished between the different grid directions. In all other cases, new numerical techniques have to be developed which are able to account for anisotropies which are represented by full tensor relative permeability functions, and which are largely independent of the choice of the grid (structured, unstructured). Moreover, upwinding strategies have to be revisited to account properly for the advection dominated behavior of multiphase flows.

In the following sections a mathematical model including the general case of anisotropic phase permeabilities is introduced and some mathematical as well as physical issues of the tensor properties of this parameters are discussed. It is important to choose a mathematical formulation which allows a numerical treatment which meets the challenges presented by the tensor properties. Further, a numerical scheme is developed which accounts for anisotropic behavior due to tensorial parameters in both the advective or gravity driven case as well as in the capillary dominated case. The scheme is based on multipoint flux approximation (MPFA) which has been derived for second order elliptic equations like Darcy's law [3, 17, 1]. There exist various types of MPFA methods where the most common one is the MPFA O-method. MPFA can be applied to unstructured grids [4] and in general shows good convergence properties for single-phase flow on quadrilateral grids [6, 32, 25, 13]. However, different kinds of MPFA methods differ with regard to convergence rates and monotonicity of the solution. Monotonicity of MPFA methods has been studied for example in [28, 29, 31]. The application of MPFA to multi-phase flow (extended Darcy) is straight forward as long as the relative permeabilities are described by scalar functions [3, 1]. In that case, the problem of evaluating the fluxes by MPFA is the same as for single-phase flow. However, if the relative permeabilities are tensors, the MPFA has to be extended to correctly account for the properties of this specific multi-phase flow regime. This applies to the simplified case neglecting capillary pressure and gravity, and becomes even more important for situations in which capillary pressure and gravity cannot be neglected. In particular, special attention is payed to a consistent upwinding strategy. The numerical method is tested on various examples, which are physically motivated and demonstrate the effects of anisotropic phase permeabilities as well as the capability of the model to account for this effects.

2. Mathematical model for two-phase flow

In the following, we describe our mathematical model for two-phase flow assuming immiscible and incompressible fluids. It is based on two conservation equations for mass, one for each of the fluid phases:

$$\phi \frac{\partial S_{\mathrm{w}}}{\partial t} + \nabla \cdot \mathbf{v}_{\mathrm{w}} - q_{\mathrm{w}} = 0, \tag{1}$$

$$\phi \frac{\partial S_{\mathrm{n}}}{\partial t} + \nabla \cdot \mathbf{v}_{\mathrm{n}} - q_{\mathrm{n}} = 0. \tag{2}$$

The wetting phase fluid is indicated by subscript w and the non-wetting phase fluid by subscript n, S is the saturation, ϕ is the porosity of the porous medium and q

a source/sink term. The momentum equations to get the phase velocities $\mathbf{v}_\mathrm{w}$ and $\mathbf{v}_\mathrm{n}$ can be simplified, applying several reasonable assumptions, to Darcy's law (e.g. [38]). It was originally derived from experimental studies for one-phase flow and extended to multi-phase flow (e.g. [35, 21])

$$\mathbf{v}_\mathrm{w} = -\frac{\mathbf{K}_{\mathrm{tot}_\mathrm{w}}}{\mu_\mathrm{w}}(\nabla p_\mathrm{w} + \varrho_\mathrm{w} g \nabla z), \tag{3}$$

$$\mathbf{v}_\mathrm{n} = -\frac{\mathbf{K}_{\mathrm{tot}_\mathrm{n}}}{\mu_\mathrm{n}}(\nabla p_\mathrm{n} + \varrho_\mathrm{n} g \nabla z). \tag{4}$$

In Equations (3) and (4) $\mathbf{K}_\mathrm{tot}$ is the total phase permeability that is usually split up into relative permeability of a phase times absolute permeability of the porous medium, μ the dynamic fluid viscosity, p the pressure and ϱ the density of the phases, and g is the gravity constant acting in z-direction. To close the system given by Equations (1) to (4) further statements are needed: The pores are entirely filled with both phases

$$S_\mathrm{w} + S_\mathrm{n} = 1, \tag{5}$$

the phase pressures are not independent but related by the capillary pressure

$$p_\mathrm{c} = p_\mathrm{n} - p_\mathrm{w}, \tag{6}$$

and the capillary pressure as well as the total phase permeabilities are modeled as functions of the saturation, which are given in terms of nonlinear constitutive relations

$$p_\mathrm{c} := p_\mathrm{c}\left(S_\mathrm{w}\right), \tag{7}$$

$$\mathbf{K}_{\mathrm{tot}_\alpha} := \mathbf{K}_{\mathrm{tot}_\alpha}\left(S_\mathrm{w}\right), \quad \alpha \in \{\mathrm{w}, \mathrm{n}\}. \tag{8}$$

Considering Darcy's law, it is obvious that the total permeability is acting like a diffusion coefficient for pressure. Thus, in the general case, it should be a symmetric tensor (real eigenvalues which are the permeabilities acting in the direction of the associated eigenvectors) and it should be positive semi-definite (which means that the eigenvalues are non-negative so that flow always takes place in the direction of decreasing potential). Further, in the fully saturated case, the total phase permeability should be the absolute permeability

$$\mathbf{K}_{\mathrm{tot}_\mathrm{w}}(1) = \mathbf{K}_{\mathrm{tot}_\mathrm{n}}(1) \overset{!}{=} \mathbf{K}, \tag{9}$$

while in the unsaturated case the medium is effectively impermeable for the corresponding phase

$$\mathbf{K}_{\mathrm{tot}_\mathrm{w}}(0) = \mathbf{K}_{\mathrm{tot}_\mathrm{n}}(0) \overset{!}{=} \mathbf{O}. \tag{10}$$

As stated before, the total phase permeability is usually split up into relative permeability of a phase and absolute permeability of the porous medium

$$\mathbf{K}_{\mathrm{tot}_\alpha} = k_{\mathrm{r}_\alpha}\mathbf{K}. \tag{11}$$

In the general case the absolute or intrinsic permeability depends on the geometric structure of the porous medium, which means it can be different in different spatial directions, and thus has to appear as a full tensor in the Darcy equations. Usually, it is assumed that the anisotropic character of flow is independent of the actual flow process and solely controlled by the porous medium and thus by the absolute permeability. Therefore, relative permeability, which includes fluid-fluid as well as fluid-fluid-solid interactions, is a scalar coefficient. However, starting from the

statements on total permeability given before, under the assumption that it consists of a relative permeability times absolute permeability, a general expression for relative permeability is given by

$$\mathbf{K}_{\mathrm{r}_\alpha}(S_\alpha) = \mathbf{K}_{\mathrm{tot}_\alpha}(S_\alpha)\,\mathbf{K}^{-1}, \tag{12}$$

which leads to

$$\mathbf{K}_{\mathrm{tot}_\alpha} = \mathbf{K}_{\mathrm{r}_\alpha}\mathbf{K}. \tag{13}$$

Examples and physical motivation for the need for both full tensor absolute as well as relative permeability have already been given before (Sec. 1) and are further extended in Section 4.

The tensorial coefficients, especially the tensorial relative permeabilities, lead to new challenges for the numerical method. These will be discussed in detail in the next section which deals with the discretization of the mathematical model. However, meeting these challenges also influences the choice of the mathematical formulation and thus some points are already mentioned here: If the direction of flow is saturation dependent via saturation dependent tensorial coefficients, the upwind direction cannot necessarily be estimated directly from the solution of the old time step. Thus, we reformulate Equations (1) to (4) into a system of equations which can be solved sequentially. It is a common assumption that the resulting pressure equation (Eq. (16)) can be treated without upwinding, because it balances total flow instead of phase flow. Further, we choose a formulation which introduces phase potentials instead of phase pressures [22]. By solving for the potentials, the gravity term is not completely moved to the right-hand side of the system of equations that has to be solved. We have observed that this can lead to a better solution behavior in the context of a sequential solution strategy where the solution for the velocity field and for the transport of the phases are decoupled. Finally, for reasons of efficiency, the formulation should ensure that the number of different transmissibilities which have to be calculated by the MPFA method is as small as possible.

With definitions of the phase mobilities $\boldsymbol{\Lambda}_\mathrm{w} = \mathbf{K}_{\mathrm{r}_\mathrm{w}}/\mu_\mathrm{w}$ and $\boldsymbol{\Lambda}_\mathrm{n} = \mathbf{K}_{\mathrm{r}_\mathrm{n}}/\mu_\mathrm{n}$, the total mobility $\boldsymbol{\Lambda}_\mathrm{t} = \boldsymbol{\Lambda}_\mathrm{w} + \boldsymbol{\Lambda}_\mathrm{n}$, and the potentials

$$\begin{aligned} \Phi_\mathrm{w} &= p_\mathrm{w} + \varrho_\mathrm{w} g\, z \\ \Phi_\mathrm{n} &= p_\mathrm{n} + \varrho_\mathrm{n} g\, z \\ \Phi_\mathrm{c} &= \Phi_\mathrm{n} - \Phi_\mathrm{w} = p_\mathrm{c} + (\varrho_\mathrm{n} - \varrho_\mathrm{w}) g\, z \end{aligned} \tag{14}$$

a total velocity can be formulated as sum of the phase velocities as

$$\begin{aligned} \mathbf{v}_\mathrm{t} =& \mathbf{v}_\mathrm{w} + \mathbf{v}_\mathrm{n} = -\boldsymbol{\Lambda}_\mathrm{w}\mathbf{K}\nabla\Phi_\mathrm{w} - \boldsymbol{\Lambda}_\mathrm{n}\mathbf{K}\nabla\Phi_\mathrm{n} \\ =& -\boldsymbol{\Lambda}_\mathrm{w}\mathbf{K}\nabla\Phi_\mathrm{w} + \boldsymbol{\Lambda}_\mathrm{n}\mathbf{K}\nabla\Phi_\mathrm{w} - \boldsymbol{\Lambda}_\mathrm{n}\mathbf{K}\nabla\Phi_\mathrm{w} - \boldsymbol{\Lambda}_\mathrm{n}\mathbf{K}\nabla\Phi_\mathrm{n} \\ =& -\boldsymbol{\Lambda}_\mathrm{t}\mathbf{K}\nabla\Phi_\mathrm{w} - \boldsymbol{\Lambda}_\mathrm{n}\boldsymbol{\Lambda}_\mathrm{t}^{-1}\boldsymbol{\Lambda}_\mathrm{t}\mathbf{K}\nabla(\Phi_\mathrm{n} - \Phi_\mathrm{w}) \\ =& \underbrace{-\boldsymbol{\Lambda}_\mathrm{t}\mathbf{K}\nabla\Phi_\mathrm{w}}_{\mathbf{v}_{\mathrm{a}_\mathrm{w}}} \underbrace{-\mathbf{F}_\mathrm{n}\boldsymbol{\Lambda}_\mathrm{t}\mathbf{K}\nabla(\Phi_\mathrm{c})}_{\mathbf{v}_\mathrm{c}} \end{aligned} \tag{15}$$

where $\mathbf{v}_{\mathrm{a}_\alpha}$ is called advective velocity of the phase α, $\mathbf{v}_\mathrm{c}$ can be called capillary velocity, although it also includes gravity effects, and $\mathbf{F}_\alpha = \boldsymbol{\Lambda}_\alpha\boldsymbol{\Lambda}_\mathrm{t}^{-1}$ is a tensorial definition of the fractional flow function of the phase α. By adding equations (1) and (2), we get a total mass balance equation. In the case of immiscible and incompressible flow this equation, which is also called pressure equation, simplifies to

$$\nabla\cdot\mathbf{v}_\mathrm{t} = \nabla\cdot(\mathbf{v}_{\mathrm{a}_\mathrm{w}} + \mathbf{v}_\mathrm{c}) = q_\mathrm{t}. \tag{16}$$

One additional equation is needed for transport of the phase and the phase mass, respectively. In case of immiscible flow we simply use one of the conservation equations for mass (Eq. (1) and (2)), which is then called saturation equation and insert phase velocities which now can be expressed in terms of $\mathbf{v}_\mathrm{a}$ and $\mathbf{v}_\mathrm{c}$:

$$\phi\frac{\partial S_\mathrm{w}}{\partial t} + \nabla\cdot(\mathbf{F}_\mathrm{w}\mathbf{v}_{\mathrm{a}_\mathrm{w}}) = q_\mathrm{w}, \tag{17}$$

$$\phi\frac{\partial S_\mathrm{n}}{\partial t} + \nabla\cdot(\mathbf{F}_\mathrm{n}\mathbf{v}_{\mathrm{a}_\mathrm{w}} + \mathbf{v}_\mathrm{c}) = q_\mathrm{n}. \tag{18}$$

3. Numerical method and multipoint flux approximations

We apply a cell-centered finite-volume method (CCFV) to Equations (16) and (17) leading to the system of equations

$$\int_{\partial V} \mathbf{v}_\mathrm{t}\cdot\mathbf{n}\,dA = \int_V q_\mathrm{t}\,dV, \tag{19}$$

$$\int_V \phi\frac{\partial S_\mathrm{w}}{\partial t}\,dV + \int_{\partial V}\mathbf{v}_\mathrm{w}\cdot\mathbf{n}\,dA = \int_V q_\mathrm{w}\,dV, \tag{20}$$

where $\mathbf{n}$ is the normal vector pointing outward of volume V at the volume boundary ∂V. Equations (19) and (20) can now be written in discrete form

$$\sum_{i=1}^{n} f_{\mathrm{tot}_i} = q_\mathrm{t}V \tag{21}$$

$$\phi\frac{\partial S_\mathrm{w}}{\partial t}V + \sum_{i=1}^{n} f_{\mathrm{w}_i} = q_\mathrm{w}V, \tag{22}$$

where f_{tot_i} is the total flux and f_{w_i} the wetting phase flux at a cell face i. According to the mathematical formulation introduced before we further split the total flux into its two components:

$$\sum_{i=1}^{n} f_{\mathrm{tot}_i} = \sum_{i=1}^{n}\left(f_{\mathrm{a}_{\mathrm{w}_i}} + f_{\mathrm{c}_i}\right) = q_\mathrm{t}V \tag{23}$$

The main challenge using the CCFV scheme now is the calculation of the numerical flux, which has to be capable of managing a tensorial relative permeability. Further, this flux should by its design be able to deal with the special challenges of advection-dominated problems. This means that the need for an upwinding concept has to be considered.

3.1. Existing numerical flux functions. The method most commonly used in finite-volume codes for groundwater or reservoir simulation is two-point flux approximation (TPFA) and descendants as numerical flux functions. However, during the last decade, the technique of multi-point flux approximations (MPFA) has been developed, supplementing the former.

Both classes of numerical flux functions are related to each other, as MPFA can be interpreted as a conceptual upgrade of TPFA. They were originally designed for flow laws like

$$\mathbf{v} = -\mathbf{K}\,\nabla p \tag{24}$$

which describes one-phase Darcy flow (for the sake of simplicity, gravity and viscosity are neglected here).

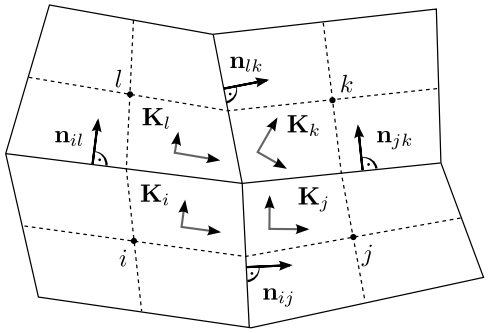

FIGURE 1. Example interaction volume for motivation of MPFA

TPFA are motivated by classical finite-difference methods. Thus the flux at face i is approximated as

$$f_i \approx T_i(p_2 - p_1), \tag{25}$$

where subscript 1 and 2 denote the two finite-volume grid cells which share interface i and T_i is the transmissibility at face i. In case of one-phase flow (Eq. (24)) it includes the absolute permeability and some geometric information. A common approach in standard finite volume simulators is to apply a harmonic average to calculate absolute permeabilities at a face i from the cell permeabilities. Compared to a arithmetic average the harmonic average naturally accounts for impermeable layers or structures. It should be mentioned that TPFA corresponds to an one-dimensional approximation of the flux leading to an important assumption for TPFA methods which is the assumption on the grid property known as K-orthogonality (see [3, 1]). If the grid is not K-orthogonal, TPFA yields an inconsistent approximation of the flux. This leads to an error in the solution which does not vanish if the grid is refined [2].

One approach to solving this problem is MPFA. There exists a variety of MPFA methods like the MPFA-O(η) method [3, 17, 32], the MPFA-U method [5], the MPFA-Z method [30], the MPFA- L method [7, 12], etc. The main aspect of MPFA methods is to increase accuracy compared to TPFA, especially in case of general non-orthogonal grids or anisotropic coefficients, by increasing the flux stencil. The various methods differ in the size of the flux stencil due to differently shaped control volumes for flux approximation. This leads to different convergence behavior and monotonicity of the methods, although it seems that there is no method, which is superior for all kinds of grids or applications. The most popular method, which is also further used in this work, is the MPFA-O method (MPFA-O(0), e.g. [1]). However, the ideas that are developed later to treat phase-dependent anisotropic parameters can be transferred to any MPFA method.

The fundamental concept of MPFA is simple: Instead of the one-dimensional approximation used by TPFA, a multi-dimensional approximation is applied:

$$f_i \approx \sum_{j \in J} t_{ij}(p_j), \tag{26}$$

where the set J includes all cells j which surround face i (e.g. 6 cells (2-d), or 18 cells (3-d) for a quadrilateral grid), and t_{ij} are called transmissibility coefficients.

For reasons of simplicity only the two-dimensional case will be further considered, although everything can be easily transferred to three dimensions. A finite-volume

grid is sketched in Figure 1 (solid lines). A dual grid (dashed lines) is constructed by drawing lines from each cell center (i, j, k, l, ...) to the midpoints of the cell faces. Every grid cell of the dual mesh now includes one vertex of the finite-volume mesh and divides its cell faces in two parts. Further, the dual grid cells, called interaction volumes, can be divided into four sub-volumes, one corresponding to every cell of the finite-volume grid that is part of the interaction volume. In analogy to the TPFA procedure, the idea is to use a linear approximation for the pressure in every sub-volume of an interaction volume. Like the TPFA, these approximations have to interpolate the nodal value of pressure at the cell centers. Furthermore, the approximation of pressure at an edge midpoint has to be the same from both sides. To preserve local conservation of fluxes it is requested that the flux leaving one control volume is equal to that entering the next one (e.g. $f_{ij} \overset{!}{=} f_{ji}$). We exemplarily write the equation describing conservation of flux along the edge from i to j

$$
\begin{aligned}
f_{ij} &\approx -\mathbf{n}_{ij}^{\mathrm{T}} \mathbf{K}_i \frac{\Gamma_{ij}}{2F_i} \left[(p_{ij} - p_i)\, \boldsymbol{\nu}_{ij}^{(i)} + (p_{il} - p_i)\, \boldsymbol{\nu}_{il}^{(i)} \right] \\
&= \mathbf{n}_{ij}^{\mathrm{T}} \mathbf{K}_j \frac{\Gamma_{ij}}{2F_j} \left[(p_{ij} - p_j)\, \boldsymbol{\nu}_{ij}^{(j)} - (p_{jk} - p_j)\, \boldsymbol{\nu}_{jk}^{(j)} \right].
\end{aligned} \tag{27}
$$

The definition of the quantities F_i, p_{ij}, $\boldsymbol{\nu}_{ij}^{(i)}$, Γ_{ij} as well as the details on the approximation of the pressure gradient are not further given here, but can be found for example in [1]. Finally, using these expressions for equality of fluxes, a system of 4 equations can be formulated for every interaction volume. This can be solved for the transmissibility matrix $\mathbf{T}$, such that

$$
\mathbf{T}\mathbf{p} = \mathbf{f}, \tag{28}
$$

where $\mathbf{p}$ is the vector of cell pressures of the four adjacent finite-volume cells sharing one interaction volume, and $\mathbf{f}$ is the vector of fluxes over the corresponding half edges. For detailed introduction and derivation of a MPFA-O method we exemplarily refer to [1, 5, 19].

In case of one-phase flow, the whole procedure of calculating the global transmissibility matrix can be accomplished in a single preprocessing step as the transmissibilities do not change during the simulation. For K-orthogonal grids, the described MPFA method reduces to TPFA with harmonic averages. However, the former can also be consistently applied to any full-tensor permeability fields on arbitrary grids. In case of multi-phase flow, the approximation of the fluxes by MPFA reduces to the form described before for one-phase flow as long as the relative permeabilities are scalars and assumed to be constant along the cell faces [3, 1].

3.2. Extension of multi-point flux approximations for multi-phase flow and tensorial relative permeabilities. The next step is the transfer of the concepts introduced before for one-phase flow (Eq. (24)) to multiphase flow (Eq. (3) and (4)) in the general case in which relative permeabilities are tensors. This means that saturation dependent quantities appear in the MPFA approximation. Thus, a fundamental difference is that the MPFA operators are saturation dependent and change with time. The transmissibilities $\mathbf{T}_{\mathrm{t}}$ (advective wetting phase flux $f_{\mathrm{a_w}}$), $\mathbf{T}_{\mathrm{n}}$ (capillary flux f_{c}) and $\mathbf{T}_{\mathrm{w}}$ (wetting phase flux f_{w}) are either related to total flow ($\mathbf{T}_{\mathrm{t}}$) or to phase flow ($\mathbf{T}_{\mathrm{n}}$, $\mathbf{T}_{\mathrm{w}}$). Especially the latter involves a careful treatment. One reason is the requirement that phase dependent quantities require an upwinding for advection-dominated problems. Another reason is that phase dependent properties like $\mathbf{F}_\alpha$ become zero if the phase is not present. Thus, the equations for

conservation of fluxes (e.g. Eq. (29)) can degenerate to the trivial statement $0 = 0$, and the system of equations that has to be solved for the transmissibility matrix would be under-determined. Further, MPFA by construction acts like a harmonic average, which means that a fluid α could never enter a cell if $S_\alpha = 0$ and therefore $\mathbf{F}_\alpha = 0$. This once more points out that an appropriate upwind scheme is important. In the case of scalar relative permeability functions, upwinding is straight forward because the direction of flow can be directly determined from the single phase transmissibilities. However, in the case of tensorial relative permeabilities, the determination of an upwind direction is challenging. Following, the multi-point flux approximations of the different flux terms ($f_{\mathrm{a_w}}$, f_{c} and f_{w}) are derived, while special emphasis is given to upwinding in case of tensorial phase-dependent coefficients.

Advective flux. Comparing Equation (24)) and Equation (15) it is obvious that the advective flux can be approximated similar to the case of one-phase flow simply by adding the total permeability into the approximation. Again, we write the equation for conservation of flux at the half edge from i to j:

$$\begin{aligned} f_{ij} &\approx -\mathbf{n}_{ij}^{\mathrm{T}} \boldsymbol{\Lambda}_{\mathrm{t}_i} \mathbf{K}_i \frac{\Gamma_{ij}}{2F_i} \left[(\Phi_{ij} - \Phi_i)\, \boldsymbol{\nu}_{ij}^{(i)} + (\Phi_{il} - \Phi_i)\, \boldsymbol{\nu}_{il}^{(i)} \right] \\ &= \mathbf{n}_{ij}^{\mathrm{T}} \boldsymbol{\Lambda}_{\mathrm{t}_j} \mathbf{K}_j \frac{\Gamma_{ij}}{2F_j} \left[(\Phi_{ij} - \Phi_j)\, \boldsymbol{\nu}_{ij}^{(j)} - (\Phi_{jk} - \Phi_j)\, \boldsymbol{\nu}_{jk}^{(j)} \right]. \end{aligned} \tag{29}$$

The total mobility $\boldsymbol{\Lambda}_{\mathrm{t}}$, which is a property of the total flux, can be easily included into the concept. It is not necessary to apply any upwinding and it can never become zero, because it is the sum of the phase mobilities. The advective flux term can thus be approximated as

$$\mathbf{f}_{\mathrm{a_w}} = \mathbf{T}_{\mathrm{t}} \boldsymbol{\Phi}_{\mathrm{w}}, \tag{30}$$

where $\mathbf{T}_{\mathrm{t}}$ is called total transmissibility and is an operator for the approximation of $\Gamma \mathbf{n}^{\mathrm{T}} \boldsymbol{\Lambda}_{\mathrm{t}} \mathbf{K} \nabla$, with Γ being the area of an half cell face. The vector $\mathbf{f}_{\mathrm{a_w}}$ contains the advective fluxes of the wetting phase corresponding to the sub-faces, while $\boldsymbol{\Phi}_{\mathrm{w}}$ holds wetting-phase potentials associated with sub-volumes (Fig. 1).

Capillary flux. The second flux term, which has to be approximated is the term f_{c}, which includes not only the total mobility tensor (Eq. (29)) but the product $\mathbf{F}_{\mathrm{n}} \boldsymbol{\Lambda}_{\mathrm{t}}$. Thus, instead of the total transmissibility a phase transmissibility is required giving the capillary flux at the half face between cell i and j as

$$\mathbf{f}_{\mathrm{c}} = \mathbf{T}_{\mathrm{n}} \boldsymbol{\Phi}_{\mathrm{c}}. \tag{31}$$

However, there exist two main problems for the calculation of the phase transmissibility $\mathbf{T}_{\mathrm{n}}$. First, the fractional flow function tensor has to be approximated at the cell face. Since the capillary flux term in this formulation includes both capillary and gravity effects, where the flux driven by gravity has advective character, an upwinding scheme is necessary ($\mathbf{F}_{\mathrm{n}} = \mathbf{F}_{\mathrm{n}}^{\mathrm{upw}}$). Second, in contrast to the total mobility, the phase mobility can become zero if the phase is at or below residual saturation. Like discussed before, this would lead to a degeneration of the system of equations which has to be solved to get the transmissibility matrix.

As mentioned upwinding can cause problems in the context of tensorial coefficients: by adding $\mathbf{F}_{\mathrm{n}}^{\mathrm{upw}}$ into Equation (29) we multiply $\boldsymbol{\Lambda}_{\mathrm{n}}$ and $\mathbf{K}$ and thus the relative permeability with the absolute permeability. So, depending on upw $= i$ or upw $= j$, one of the products of relative and absolute permeability (from cell i or j) is a product where both permeabilities come from the same cell whereas

the other product is a mixed product. For the latter case it is not guaranteed that the total permeability satisfies the criteria discussed before (sec. 2). Even if both, the absolute permeability as well as the relative permeability are symmetric and positive definite, the total permeability resulting from the mixed product does not have to satisfy this properties, because the principal directions could be completely different. An entirely unphysical behavior could be the result, for example a flow in the direction of increasing potential. Furthermore, we multiply $\mathbf{\Lambda}_{\mathrm{t}}^{\mathrm{T}}$ and $\mathbf{\Lambda}_{\mathrm{t}}$, which could result in similar problems although the total mobility is supposed to be quite smooth and numerically easy to handle.

The solutions to these problems are quite simple. Instead of upwinding the whole mobilities only the quantity that shows hyperbolic character, namely the saturation, is used in the upwinding procedure. Accordingly, we write

$$\mathbf{F}_{\mathrm{n}_{ij}} = \mathbf{F}_{\mathrm{n}_{ij}}^{\mathrm{upw}} = \mathbf{F}_{\mathrm{n}_{ij}}\left(S^{\mathrm{upw}}\right). \tag{32}$$

We assumed before that we do not need to apply an upwinding scheme on the total mobility $\mathbf{\Lambda}_{\mathrm{t}}$ to calculate the advective flux. To be consistent we also use this assumption for the other flux terms. For the capillary flux this means that only the fractional flow function is calculated from an upwind saturation S^{upw}. The determination of an upwind direction which is quite simple for scalar fractional flow functions however is nontrivial for tensor functions. The reason is that a tensor coefficient like $\mathbf{F}$ can lead to phase normal flux in opposite direction than the total flux as well as the phase potential difference of two neighboring cells. We therefore suggest the following procedure:

(1) Calculate the phase transmissibilities without upwinding.
(2) Calculate phase fluxes using the pressure field of the old time step (this is reasonable as in the sequential solution strategy the capillary flux term is also assumed to be known from the old time step and thus completely moved to the right hand side).
(3) Calculate upwind fractional flow functions, where the directions of the previously calculated phase fluxes determine the upwind direction.

To address the second problem of possibly ill-posed linear systems during the calculation of the phase transmissibilities, we suggest the following: the coefficients $f_{\mathrm{c}_{ij}}$ of the vector $\mathbf{f}_{\mathrm{c}}$ are given by

$$f_{\mathrm{c}_{ij}} = \Gamma_{ij}\mathbf{n}_{ij}^{\mathrm{T}}\mathbf{F}_{\mathrm{n},\varepsilon_{ij}}\mathbf{n}_{ij}f_{\mathrm{c,mpfa}_{ij}}, \tag{33}$$

where $f_{\mathrm{c,mpfa}_{ij}}$ are the coefficients of a flux vector $\mathbf{f}_{\mathrm{c,mpfa}}$,

$$\mathbf{f}_{\mathrm{c,mpfa}} = \mathbf{T}_{\mathrm{n}}\mathbf{\Phi}_{\mathrm{c}}, \tag{34}$$

with the transmissibility $\mathbf{T}_{\mathrm{n}}$ calculated from flux balances like

$$\begin{aligned} f_{\mathrm{c,mpfa}_{ij}} &\approx -\mathbf{n}_{ij}^{\mathrm{T}}\mathbf{F}_{\mathrm{n,mpfa}_{ij}}\mathbf{\Lambda}_{\mathrm{t}_i}\mathbf{K}_i\frac{\Gamma_{ij}}{2F_i}\left[\left(\Phi_{ij}-\Phi_i\right)\boldsymbol{\nu}_{ij}^{(i)}+\left(\Phi_{il}-\Phi_i\right)\boldsymbol{\nu}_{il}^{(i)}\right] \\ &= \mathbf{n}_{ij}^{\mathrm{T}}\mathbf{F}_{\mathrm{n,mpfa}_{ij}}\mathbf{\Lambda}_{\mathrm{t}_j}\mathbf{K}_j\frac{\Gamma_{ij}}{2F_j}\left[\left(\Phi_{ij}-\Phi_j\right)\boldsymbol{\nu}_{ij}^{(j)}-\left(\Phi_{jk}-\Phi_j\right)\boldsymbol{\nu}_{jk}^{(j)}\right]. \end{aligned} \tag{35}$$

To ensure that the system of flux balances can always be solved for a transmissibility matrix we now add the condition

$$\mathbf{F}_{\mathrm{n,mpfa}} = \begin{cases} \mathbf{I}, & \text{if } \lambda\left(\mathbf{F}_{\mathrm{n,mpfa}}\right) < \varepsilon \\ \mathbf{F}_{\mathrm{n}}, & \text{else} \end{cases}, \qquad \mathbf{F}_{\mathrm{n},\varepsilon} = \begin{cases} \mathbf{I}, & \text{if } \lambda\left(\mathbf{F}_{\mathrm{n},\varepsilon}\right) \geq \varepsilon \\ \mathbf{F}_{\mathrm{n}}, & \text{else} \end{cases}. \tag{36}$$

which ensures that the fractional flow function tensor is removed from the transmissibility calculation if one of its eigenvalues $\lambda(\mathbf{F}_{\mathrm{n}})$ is smaller than a certain threshold ε.

Wetting phase flux. From Equation (17) we see that the wetting phase flux has the same structure than the capillary flux. Thus, the MPFA approximation can be written by substituting the capillary potential in Equation (34) by the wetting phase potential, the non-wetting phase fractional flow functions of Equations (33) and (35) by the wetting phase fractional flow function, and the capillary flux by the advective flux:

$$f_{\mathrm{w}_{ij}} = \Gamma_{ij}\mathbf{n}_{ij}^{\mathrm{T}}\mathbf{F}_{\mathrm{w},\varepsilon_{ij}}\mathbf{n}_{ij}f_{\mathrm{w,mpfa}_{ij}}, \tag{37}$$

$$\mathbf{f}_{\mathrm{w,mpfa}} = \mathbf{T}_{\mathrm{w}}\mathbf{\Phi}_{\mathrm{w}}. \tag{38}$$

The crucial points concerning phase quantities in the MPFA method have already been discussed for the approximation of the capillary flux. It is obvious that the same problems occur for the approximation of the phase flux. Thus, we approximate the wetting phase fractional flow function tensor at a face ij as

$$\mathbf{F}_{\mathrm{w}_{ij}} = \mathbf{F}^{\mathrm{upw}}_{\mathrm{w}_{ij}} = \mathbf{F}_{\mathrm{w}_{ij}}\left(S^{\mathrm{upw}}\right). \tag{39}$$

Compared to the capillary flux, which has to be determined for the solution of the pressure equation, the wetting phase flux is needed to solve the saturation transport equation. This means, that in a sequential solution strategy the pressure field of the new time step is already known. Thus, the scheme to determine the upwind directions given for the capillary flux is also applied for the phase flux, but substituting the pressure of the old time step in step (2) by the pressure of the new time step.

As stated before, in the original MPFA method for single-phase flow the transmissibilities have to be calculated only once in a preprocessing step and do not change during a simulation. Of course, this is different if a saturation dependent quantity like mobility is included into the transmissibility. Additionally, different terms like advective term, gravity or capillary pressure term need different treatment leading to different MPFA operators or transmissibilities, respectively. In the proposed method we need to calculate three different transmissibilities to calculate the different fluxes (advective flux, capillary flux, wetting/non-wetting phase flux). Further, four additional transmissibilities are needed to determine the upwind directions (wetting and non-wetting phase direction for each potential and saturation transport calculation) leading to seven transmissibility calculations for each grid vertex and each time step. Depending on the flow problem, it can be reasonable to determine the upwind direction only once each time step (for both equations). This would reduce the transmissibility calculations to five, but could also reduce accuracy. To make further statements about efficiency different methods have to be investigated. One alternative can be found in [24], where the authors approximate the phase fluxes using an approximate Riemann solver.

Some remarks on upwinding. There exists one crucial difficulty for upwinding in presence of tensor coefficients like relative permeability, which are saturation dependent and therefore change in time. Except for the case where it can be assumed that the direction of the total permeability does not change with saturation but only the absolute values, it is not possible to base the upwinding decision on the solution of the old time step. However, in the general case the direction of

tensorial total permeabilities is saturation dependent. Thus, the direction of flow can change from one time step to another as saturation changes.

The challenge of an MPFA concept for multi-phase flow is to avoid upwinding whenever this is possible and if it can not be avoided to find a solution that is sufficiently accurate and computationally efficient. If Equations (1) and (2) are solved simultaneously applying a fully implicit scheme the only way out of the upwinding dilemma seems to be the following: First, calculate transmissibility matrices for every possible upwind combination for every interaction volume ($2e4 = 16$ combinations = 16 transmissibility matrices for each interaction volume (2-d)). Second, find and apply kind of heuristic criteria to decide which is the most likely combination. It is obvious, that on the one hand formulation of reasonable criteria can be difficult and on the other hand recalculation of the transmissibilities is very costly (already in 2-d). This consideration is the motivation to use a different model formulation. The reformulation into one equation for potentials and one equation for transport of saturation accompanied with a sequential solution strategy allows for decoupling of some steps. Thus, upwinding decisions described before are not based on the old solution, but always on information of the new time step that is already available. Of course, this concept also includes some necessary assumptions:

- It is common to use the total mobility without any upwinding because it is a property of the total flow which uses to behave quite smooth within the model domain. We assume that this still holds for tensorial total mobilities. This allows to calculate the advective flux (Eq. (29) without any upwinding.
- The capillary as well as the gravity part are assumed to be known from the old time step, and put to the right hand side of the system of equations. This is common if a pressure (or potential) equation and a transport equation (e.g. for saturation) are solved sequentially. Thus, it is assumed that it is sufficient to base the upwind decision for this flux term also on the solution of the old time step.
- In the procedure to determine the upwind directions, cell values of the phase quantities are used for transmissibility calculation. Thus, it is assumed that the upwinding has no influence on the direction of flow but only on the amount of fluid that crosses a cell face.
- We apply saturation upwinding instead of direct upwinding of the relative permeability. In the homogeneous case this results in the same relative permeability than relative permeability upwinding. However, saturation upwinding also ensures that heterogeneous anisotropy is accounted for in the flux approximation and that unphysical fluxes (e.g. in opposite direction to the potential gradient) are avoided.

4. Numerical Examples

In this section different numerical experiments are performed and the results are shown to demonstrate and test the capabilities of the proposed numerical method. In a first part, we use a diagonal relative permeability tensor derived for a horizontally layered system. It has been shown for example in [10, 18] that in such systems layers of different entry pressures can lead to anisotropic relative permeabilities at a larger scale. In the second part, we consider full tensor relative permeabilities. If we still think of a layered system a full tensor could result from an upscaling if the layers are not horizontal but rotated. Of course there are also other effects that might cause anisotropy of large scale relative permeability functions. Although the example we present is not the result of an upscaling, but artificially generated, it

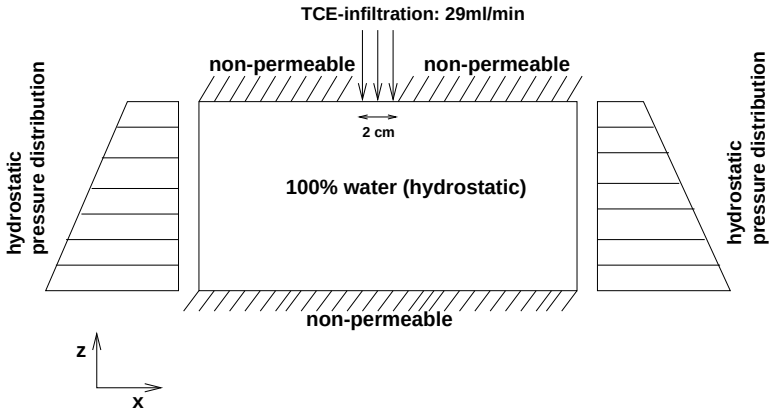

FIGURE 2. Setup of the infiltration experiment.

demonstrates the effects of a full relative permeability tensor as well as it provides a meaningful test for our numerical method. We do not compare MPFA and TPFA as it has already been shown for simpler cases that TPFA leads to inaccuracy if it is used on unstructured grids or with anisotropic parameters (e.g. [12]). We further remark that all numerical test examples discussed in the following use symmetric tensors for the total phase permeability. However, the presented algorithm does not require this symmetry.

4.1. Diagonal relative permeability tensor from upscaling. The first test example is taken from [18], where flow experiments and numerical simulations of a horizontally layered system are compared. The layers consist of three different soil types (permeability $\mathbf{K}_{\text{fine}} = 6.38 \times 10^{-11}$, $\mathbf{K}_{\text{medium}} = 1.22 \times 10^{-10}$, $\mathbf{K}_{\text{coarse}} = 2.55 \times 10^{-10}$, porosity $\Phi = 0.38$). The setup is shown in Figure 2. A DNAPL (Denser Non-Aqueous-Phase Liquid, here TCE) is injected from the top into a domain of 1.2 m length and 0.5 m height. The upper and lower boundaries are closed for flow, except for the injection area. On the right as well as on the left boundary a hydrostatic pressure profile is assumed. The domain is initially fully water saturated. The location of the layers as well as the entry pressures of the differently permeable layers (entry pressure $p_{\text{d}_{\text{fine}}} = 882.9$, $p_{\text{d}_{\text{medium}}} = 539.55$, $p_{\text{d}_{\text{coarse}}} = 353.16$) are shown in Figure 3. On this scale (fine scale) Brooks-Corey type functions are used for capillary pressure-saturation and relative-permeability-saturation relations [11]. The capillary pressure-saturation curves of the different layers are correlated to the permeabilities according to a Leverett J-function [26]. The upscaled capillary pressure function for this system is plotted in Figure 4a, the effective relative permeability functions for the two fluids in different coordinate directions are shown in Figure 4b. Both kinds of effective coarse scale functions are derived from capillary equilibrium conditions. The steady state fluid distributions (each representing one point on each graph shown in Figure 4) are obtained from a static site-percolation model (see e.g. [37]) and used to calculate a coarse scale saturation for a given equilibrium capillary pressure. The relative permeability functions are calculated from the steady state saturation distributions applying an upscaling concept for single-phase flow [16]. The simulated time is 1 hour while the injection is stopped after ~ 50 minutes. For a more detailed description of the problem setting and the upscaling method we refer to [18].

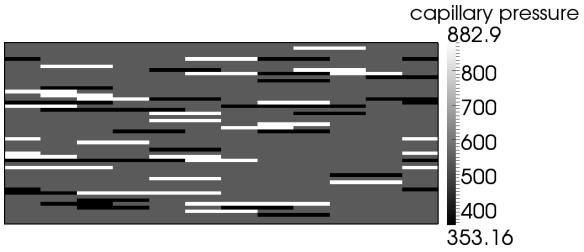

FIGURE 3. Model domain with the discrete lenses showing the different entry pressures.

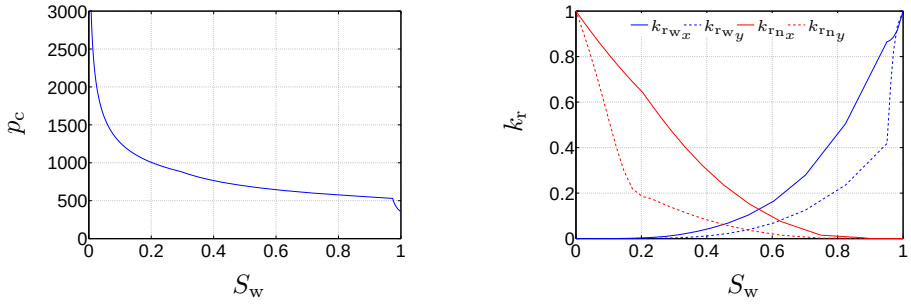

(A) capillary pressure (B) relative permeability

FIGURE 4. Coarse scale constitutive relations from upscaling (see [18]).

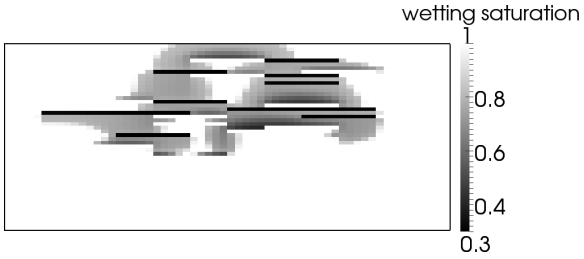

FIGURE 5. Saturation distributions of example 1 calculated with resolved lenses.

First, we compare the results using the upscaled, diagonal relative permeability tensor function with the results modeling the discrete lenses (no anisotropy on the scale of the single layers). For better comparability we use the same numerical methods (Cell Centered Finite Volumes with MPFA), but for scalar relative permeability functions in the discrete case. The grid consists of 60×50 elements which allows the resolution of the lenses. The saturation distribution resulting from the simulation of the discrete system shown in Figure 5 is in good agreement with the results presented in [18] for the real experiment as well as for the numerical simulation. The simulations using the upscaled tensor functions are carried out on different grid types which are shown in Figures 6a to 6d. The unstructured grids (B-D) are chosen to be no longer K-orthogonal, which means that the normal vectors of the cell faces do not have to be in alignment with the directions of the

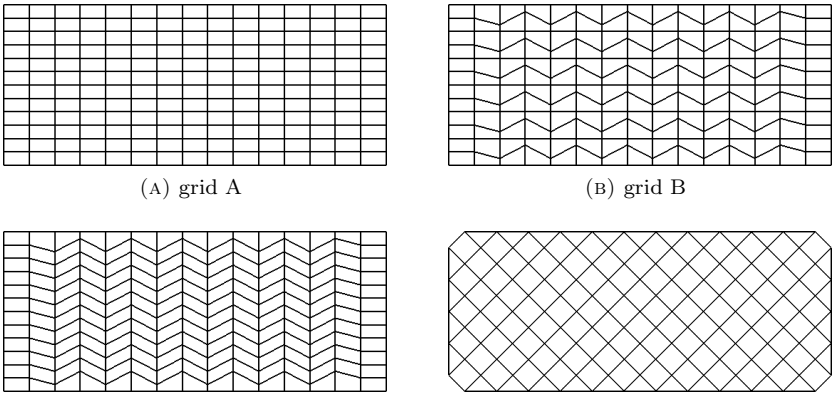

(A) grid A (B) grid B

(C) grid C (D) grid D

FIGURE 6. Different structured and unstructured grids used to test the mpfa method.

anisotropy. Like for the discrete calculations grids consisting of 60×50 elements (grids A-C) and approximately 60×50 elements (grid D, 3082 elements) respectively are used. In particular, the same amount of TCE is injected. The results are shown in Figure 7a (structured), and Figures 7b to 7d (unstructured). For better comparison, the following spatial moments are calculated:

$$m_0 = \int_V \Phi S_\mathrm{n} \, dV, \tag{40}$$

$$\mathbf{m}_1 = \frac{1}{m_0} \int_V \Phi S_\mathrm{n} \mathbf{x} \, dV, \tag{41}$$

$$\mathbf{M}_2 = \frac{1}{m_0} \int_V \Phi S_\mathrm{n} (\mathbf{x} - \mathbf{m}_1)(\mathbf{x} - \mathbf{m}_1)^\mathrm{T} \, dV, \tag{42}$$

where m_0 is the non-wetting phase volume in the system, $\mathbf{m}_1$ is the center of gravity of the non-wetting phase plume, and $\mathbf{M}_2$ is the matrix of variances and covariances of the plume related to its center of gravity. The transformation of $\mathbf{M}_2$ into a diagonal matrix gives the variances along the main axis of the plume (assuming an elliptical approximation). Accordingly, the spatial extent of the plume can in average be approximated by the square root of the diagonalized variance matrix. For the horizontally layered system, the main axis are in horizontal and vertical direction. The results of the spatial moments analysis are plotted in Figure 8. Qualitatively, the main features of the discrete model are captured well. This demonstrates that the proposed numerical model accounts for the anisotropic parameters. However, quantitatively the horizontal spreading of the infiltrating non-wetting phase is underestimated (Fig. 8a), whereas the vertical spreading is overestimated (Fig. 8b). This might be due to gravity effects, but is not further investigated here as the upscaling itself is not part of this work. Further, only negligible differences can be observed in the moment analysis using the different grids. The total mass which is injected is not plotted in Figure 8 but is equal for the compared simulations. Differences between Figure 7a to 7c and Figure 7d are mainly caused by a different

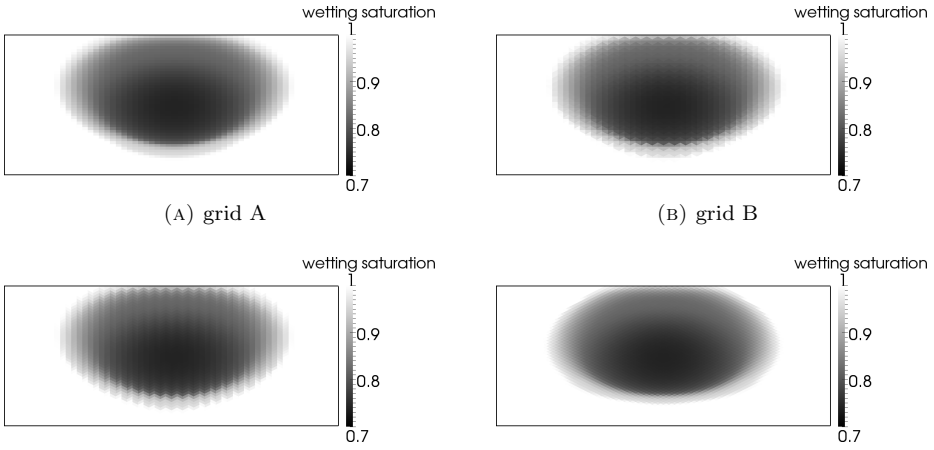

(A) grid A (B) grid B

(C) grid C (D) grid D

FIGURE 7. Saturation distributions of example 1 using the upscaled coarse scale functions on the different grids shown in Figures 6a-6d.

propagation along the upper boundary, where triangles instead of quadrilaterals are used for grid D. The use of isotropic effective relative permeability functions has been tested, but the results are not shown here. It can be observed that the anisotropic distribution behavior of the discrete system is mainly caused by the different entry pressures of the lenses and can not be covered just by a tensorial absolute permeability. This is in accordance with the results of [18].

In a next test, we keep the domain of the previous example, but neglect gravity ($g = 0$) and apply a diagonal pressure gradient comparable to a classical five-spot problem. The grid is a cartesian grid consisting of 120×50 elements. We place an injection well at the lower left corner and a production well at the upper right corner and close all boundaries for flow. The shape of the domain has to remain rectangular instead of quadratical, what is usually the case for a five-spot problem, because the upscaled functions are derived for the whole rectangular domain. Still the effect is a diagonal gradient which is not aligned with the grid axis. In a second test we again close all boundaries and place injection wells at the lower left as well as at the upper right corner and production wells at the lower right and upper left corner. The sources are chosen in such a way that the pressure gradient is small and capillary forces are not negligible. This should eliminate effects which may not be captured by the upscaling method used in [18]. The results are shown in Figures 9a and 9b. In both cases the results using the upscaled relative permeability tensor functions are in good agreement with the fine scale simulations. Further, there is no difference between the non-wetting phase distributions of the two cases on the lower left part of the domain. This shows that the gradient is approximated well independent of the direction of the gradient in relation to the orientation of the grid axis (structured grid).

4.2. Full relative permeability tensor. So far, all numerical test examples use a diagonal tensor relative permeability derived from upscaling. Rotation of the orientation of the lenses (Fig. 3) would result in non-diagonal, full tensor relative permeability functions. However, upscaling of two-phase flow parameters is not

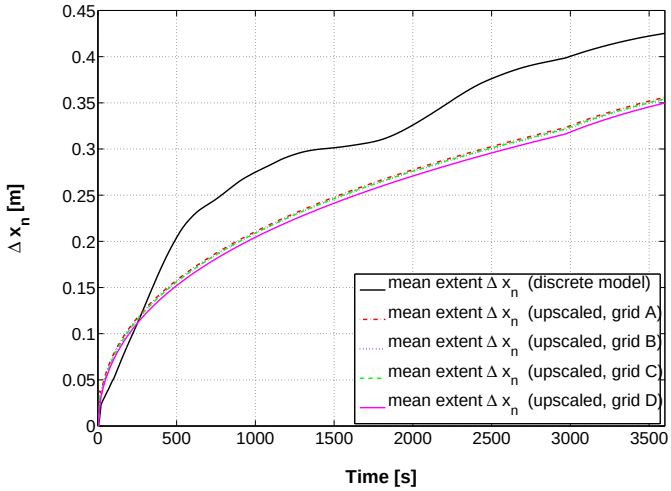

(A) averaged extent of the non-wetting fluid distribution in horizontal direction (standard deviation × 2 - from 2nd spatial moment)

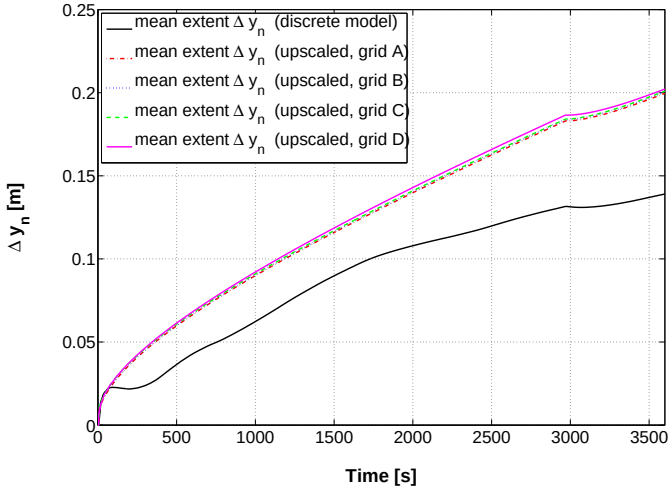

(B) averaged extent of the non-wetting fluid distribution in vertical direction (standard deviation × 2 - from 2nd spatial moment)

FIGURE 8. Comparison of the results shown in Figures 5, 7a-7d using spatial moment analysis.

part of this work. Thus, we use the same experimental setup than for the diagonal tensor relative permeability functions (Fig. 2) but replace the relative permeability function by the function derived in [24] which results from the consideration of vertically segregated upscaling:

$$\mathbf{K}_{\mathrm{r}_\alpha} = S_\alpha \begin{pmatrix} 1 & \frac{0.9}{2\pi S_\alpha}(1-\cos(2\pi S_\alpha)) \\ \frac{0.9}{2\pi S_\alpha}(1-\cos(2\pi S_\alpha)) & S_\alpha^{\frac{1}{2}} \end{pmatrix}, \qquad \alpha \in \{\mathrm{w},\mathrm{n}\}\,. \tag{43}$$

(A) Source in the lower left corner

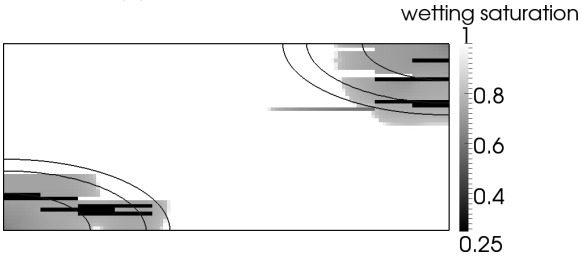

(B) Sources in the lower left and upper right corner

FIGURE 9. Saturation distributions of the discrete lens model applying a diagonal pressure gradient. The solid lines are the contours of the saturation distributions resulting from the upscaled tensor functions.

Although this function is physically motivated, it has no physical meaning in the sense it is used here. It can be seen as any artificially generated full tensor relative permeability function to test the capabilities of the numerical model as well as to show that there can be a notable influence of off-diagonal effects. Additionally, compared to the previous examples where only the anisotropy ratio is saturation dependent, the direction of the eigenvectors of the matrices resulting from Equation (43) is saturation dependent. The simulations are carried out on two different grids, grid A (Fig. 6a, structured) and grid B (6b, unstructured) which again consist of 60×50 elements. The results are plotted in Figures 10a and 10b. Comparing these results with the results of the diagonal tensor case (Fig. 7a-7d) it is obvious that there can be a huge influence of the off-diagonal effects. The infiltrating non-wetting phase only spreads into the left side of the domain, whereas the spreading in the diagonal case is symmetric. The results are further independent of the two different kinds of grids chosen for these calculations.

5. Summary/Conclusions

Upscaling of two-phase flow in anisotropically structured porous media can result in anisotropic large scale properties. It is common to use absolute permeability tensors, but it has been shown that there exists also an anisotropy in the multi-phase flow behavior. Thus, it is obvious that upscaling should also result in anisotropic multi-phase properties, namely anisotropic relative permeabilities.

In this work we have considered the general case of an anisotropic, full tensor phase permeability and have discussed the consequences for a splitting into the product of absolute and relative phase permeability. The case of the product of

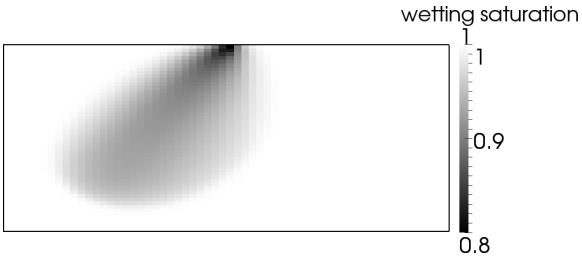

(A) grid A

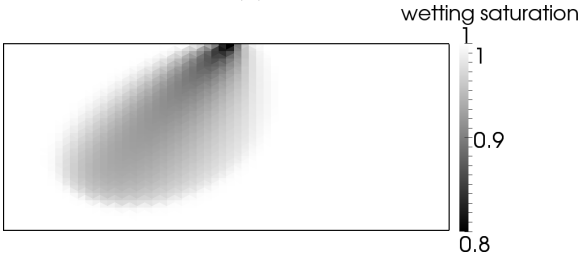

(B) grid B

FIGURE 10. Saturation distributions of example 3 on grid A (Fig. 6a) and B (Fig. 6b).

two full tensors (instead of a scalar and a tensor, what is usually assumed) requires new concepts to solve the model equations numerically. We have introduced a new numerical method using a cell centered finite volume technique with multipoint flux approximation, which includes a special upwinding strategy to properly account for the effects of the full tensor relative permeability functions.

For validation, different numerical experiments have been carried out and it has been shown that the proposed method properly accounts for the anisotropy, also in the case of a full (rotated) tensor. Further, the examples show that different physical effects of two-phase flow, which means also capillary pressure and gravity effects, are accounted for in a meaningful way and independent of the choice of the (quadrilateral) numerical grid. The performance of the method is still sufficient, although not as good as in the case of scalar relative permeabilities. The reason is the more expensive upwinding procedure. However, the costs to determine the upwind direction do not increase if the dimension is increased, which means the costs of the upwinding become less important for three-dimensional problem settings.

If we think about a coarse scale model as a combination of an upscaling method and a suitable numerical scheme, it is obvious that a wrong coarse-scale solution compared to a given (averaged) fine-scale solution can either be introduced by the upscaling or by the numerical scheme or by both of them. So far, upscaling methods resulting in tensorial phase-dependent parameters could not be treated numerically in a proper way. This makes it difficult to validate the quality of the upscaling part alone because comparable results are those of the combined coarse scale model. However, the development of a suitable numerical method can only be the first step. The next step must be to use the method for a closer investigation of different upscaling concepts, in order to obtain a better understanding of the effects of anisotropic structures on different scales.

Acknowledgments

The authors would like to thank the German Research Foundation (DFG) for financial support of the project within the Cluster of Excellence in Simulation Technology (EXC 310/1) at the University of Stuttgart and the International Research Training Group NUPUS.

References

[1] I. Aavatsmark. An introduction to multipoint flux approximations for quadrilateral grids. *Computational geosciences*, 6(3-4):405–432, 2002.

[2] I. Aavatsmark. Interpretation of a two-point flux stencil for skew parallelogram grids. *Computational geosciences*, 11(4):199–206, 2007.

[3] I. Aavatsmark, T. Barkve, Ø. Bøe, and T. Mannseth. Discretization on non-orthogonal, quadrilateral grids for inhomogeneous anisotropic media. *Journal of computational physics*, 127:2–14, 1996.

[4] I. Aavatsmark, T. Barkve, Ø. Bøe, and T. Mannseth. Discretization on unstructured grids for inhomogeneous, anisotropic media. Part I: Derivation of the methods. Part II: Discussion and numerical results. *SIAM Journal on scientific computing*, 19(5):1700–1736, 1998.

[5] I. Aavatsmark and G. T. Eigestad. Numerical convergence of the mpfa o-method and u-method for general quadrilateral grids. *International journal for numerical methods in fluids*, 51(9-10):939–961, 2006.

[6] I. Aavatsmark, G. T. Eigestad, and R. A. Klausen. Numerical convergence of the MPFA O-method for general quadrilateral grids in two and three dimensions. In D. N. Arnold, P. B. Bochev, R. B. Lehoucq, R. A. Nicolaides, and M. Shashkov, editors, *Compatible spatial discretizations*, volume 142 of *IMA Volumes in mathematics and its applications*, pages 1–21. Springer, New York, 2006.

[7] I. Aavatsmark, G. T. Eigestad, B. T. Mallison, and J. M. Nordbotten. A compact multipoint flux approximation method with improved robustness. *Numerical methods for partial differential equations*, 24(5):1329–1360, 2008.

[8] M. Acosta, C. Merten, Eigenberger, H. Class, R. Helmig, B. Thoben, and H. Mller-Steinhagen. Modeling non-isothermal two-phase multicomponent flow in the cathode of pem fuel cells. *Journal of power sources*, 2(2):1123–1141, 2006.

[9] F. Barbir. *PEM fuel cells: Theory and practice*. Elsevier, Academic press, Burlington, 2005.

[10] C. Braun, R. Helmig, and S. Manthey. Determination of constitutive relationships for two-phase flow processes in heterogeneous porous media with emphasis on the relative permeability-saturation-relationship. *Journal of contaminant hydrology*, 76(1-2):47–85, 2005.

[11] R. H. Brooks and A. T. Corey. Hydraulic properties of porous media. *Hydraulic paper*, (3), Colorado State University, 1964.

[12] Y. Cao, R. Helmig, and B. Wohlmuth. Geometrical interpretation of the multipoint flux approximation l-method. *International journal for numerical methods in fluids*, 60(11):1173–1199, 2009.

[13] Y. Cao, R. Helmig, and B. Wohlmuth. Convergence of the multipoint flux approximation l-method for homogeneous media on uniform grids. *Numerical methods for partial differential equations*, 27(2):329–350, 2011.

[14] Y. Chen and L. J. Durlofsky. Efficient incorporation of global effects in upscaled models of two-phase flow and transport in heterogeneous formations. *Multiscale modeling & simulation*, 5(2):445–475, 2006.

[15] H. Class, A. Ebigbo, R. Helmig, H. K. Dahle, J. M. Nordbotten, M. A. Celia, P. Audigane, M. Darcis, J. Ennis-King, Y. Fan, B. Flemisch, S. E. Gasda, M. Jin, S. Krug, D. Labregere, A. Naderi Beni, R. J. Pawar, A. Sbai, S. G. Thomas, L. Trenty, and L. Wei. A benchmark study on problems related to CO_2 storage in geologic formations: Summary and discussion of the results. *Computational geosciences*, 13(4):409–434, 2009.

[16] L. J. Durlofsky. Numerical calculation of equivalent grid block permeability tensors for heterogeneous porous media. *Water resources research*, 27(5):699–708, 1991.

[17] M. G. Edwards and C. F. Rogers. Finite volume discretization with imposed flux continuity for the general tensor pressure equation. *Computational geosciences*, 2(4):259–290, 1998.

[18] H. Eichel, R. Helmig, I. Neuweiler, and O. A. Cirpka. Upscaling of two-phase flow processes in porous media. In D. B. Das and S. M. Hassanizadeh, editors, *Upscaling multiphase flow in porous media*, pages 237–257. Springer, 2005.

[19] G. T. Eigestad and R. A. Klausen. On the convergence of the multi-point flux approximation o-method: Numerical experiments for discontinuous permeability. *Numerical methods for partial differential equations*, 21(6):1079–1098, 2005.
[20] K. Erbertseder, J. Reichold, R. Helmig, P. Jenny, and B. Flemisch. A coupled discrete/continuum model for describing cancer therapeutic transport in the lung. *PLoS*, 2011 (submitted).
[21] R. Helmig. *Multiphase flow and transport processes in the subsurface: A contribution to the modeling of hydrosystems*. Springer, Berlin, 1997.
[22] H. Hoteit and A. Firoozabadi. Numerical modeling of two-phase flow in heterogeneous permeable media with different capillarity pressures. *Advances in water resources*, 31(1):56–73, 2008.
[23] A. Humphrey J. Smith J. Interstitial transport and transvascular fluid exchange during infusion into brain and tumor tissue. *Microvascular research*, 73(1):58–73, 2007.
[24] E. Keilegavlen, J. M. Nordbotten, and A. Stephansen. Tensor relative permeabilities: Origins, modeling and numerical discretization. *International journal of numerical analysis and modeling*, 2011.
[25] R. A. Klausen and R. Winther. Convergence of multipoint flux approximations on quadrilateral grids. *Numerical methods for partial differential equations*, 22(6):1438–1454, 2006.
[26] M. C. Leverett. Capillary behavior in porous solids. *Transactions of the american institute of mining and metallurgical engineers*, 142:152–169, 1941.
[27] Y. Chen Y. Li. Local-global two-phase upscaling of flow and transport in heterogeneous formations. *Multiscale modeling & simulation*, 8(1):125–153, 2009.
[28] J. M. Nordbotten and I. Aavatsmark. Monotonicity conditions for control volume methods on uniform parallelogram grids in homogeneous media. *Computational geosciences*, 9(1):61–72, 2005.
[29] J. M. Nordbotten, I. Aavatsmark, and G. T. Eigestad. Monotonicity of control volume methods. *Numerische mathematik*, 106(2):255–288, 2007.
[30] J. M. Nordbotten and G. T. Eigestad. Discretization on quadrilateral grids with improved monotonicity properties. *Journal of computational physics*, 203(2):744–760, 2005.
[31] M. Pal and M. G. Edwards. Non-linear ux-splitting schemes with imposed discrete maximum principle for elliptic equations with highly anisotropic coefcients. *International journal for numerical methods in fluids*, 66(3):299–323, 2011.
[32] M. Pal, M. G. Edwards, and A. R. Lamb. Convergence study of a family of flux-continuous, finite-volume schemes for the general tensor pressure equation. *International journal for numerical methods in fluids*, 51(9-10):1177–1203, 2006.
[33] G. E. Pickup and K.S. Sorbie. The scaleup of two-phase flow in porous media using phase permeability tensors. *SPE Journal*, (28586):369–381, 1996.
[34] N. Saad, A. S. Cullick, M. M. Honarpour, and Mobil E&P Technical Center. Effective relative permeability in scale-up and simulation. *SPE*, (29592), 1995.
[35] A. Scheidegger. *The physics of flow through porous media*. University of Toronto Press, 3d edition, 1974.
[36] V. B. Serikov. Porous phase model of the lung interstitial fluid motion. *Microvascular research*, 42(1):1–16, 1991.
[37] D. Stauffer. *Introduction to percolation theory*. Taylor & Francis, London, 1985.
[38] S. Whitaker. *The method of volume averaging*. Kluwer, Dordrecht, 1999.

IWS, Department of Hydromechanics and Modeling of Hydrosystems, University of Stuttgart,, Pfaffenwaldring 61, 70569 Stuttgart, Germany

E-mail: `markus.wolff@iws.uni-stuttgart.de and bernd.flemisch@iws.uni-stuttgart.de and rainer.helmig@iws.uni-stuttgart.de`

Centre for Integrated Petroleum Research, University of Bergen,, P.O.Box 7800, NO-5020 Bergen, Norway

E-mail: `ivar.aavatsmark@cipr.uib.no`